Published February 1, 2003. Distribution restricted to Sponsors until May 1, 2003.

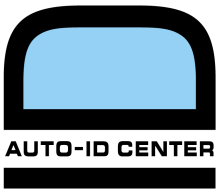

TECHNICAL REPORT

Vibratory Assembly Update: Part Transportation Mechanics Analysis

Kashif Khan, Sanjay Sarma

AUTO-ID CENTER MASSACHUSETTS INSTITUTE OF TECHNOLOGY, 77 MASSACHUSETTS AVENUE, BLDG 3-449, CAMBRIDGE, MA 02139-4307, USA

ABSTRACT

Bulk part manipulation using vibrating surfaces is an effective technique for economically transporting and feeding small parts such as electronic devices. Micro-fabricated devices have often used robotic gripping and manipulation for transportation and assembly of integrated circuits into electronic devices. The vibratory technique holds the promise for improving production economics over traditional non-bulk transportation techniques such as robotic part handling, while providing greater flexibility than other bulk transportation methods.

In this paper we present the mechanics of microscopic vibratory parts handling. As parts become smaller, surface forces and fluid mechanical effects become prominent compared to the gravitational and inertia effects that predominate at macroscopic scales. We consider the growth of adhesion and aerodynamic damping forces at the smaller operating scales, and describe the prominent vibratory feeding techniques available for microscopic scale parts and the modifications they may require to account for the presence of surface forces.

Published February 1, 2003. Distribution restricted to Sponsors until May 1, 2003.

TECHNICAL REPORT

Vibratory Assembly Update: Part Transportation Mechanics Analysis

Biography

Kashif A. Khan
Doctoral candidate

Kashif A. Khan is a Doctoral candidate in the Department of Aeronautics and Astronautics at MIT. He has received a Bachelor's in Mechanical Engineering from the University of Engineering and Technology, Lahore, Pakistan, and a Master's in Aeronautics and Astronautics from MIT. At MIT, he has researched Air traffic Management Systems for Reusable Launch Vehicles, as well as Air traffic Simulation Models. His current research focus at the Auto-ID Center is on future packaging concepts for RFID tags.

Sanjay E. Sarma
Research Director

Sanjay Sarma received his Bachelors from the Indian Institute of Technology, his Masters from Carnegie Mellon University and his PhD from the University of California at Berkeley. In between degrees he worked at Schlumberger Oilfield Services in Aberdeen, UK, and at the Lawrence Berkeley Laboratories in Berkeley, California. Prof. Sarma's Masters thesis was in the area of operations research and his PhD was in the area of manufacturing automation. From 1995 to 1999, Dr. Sarma was an Assistant Professor in the Department of Mechanical Engineering at the Massachusetts Institute of Technology. He is now an associate professor.

TECHNICAL REPORT

Vibratory Assembly Update: Part Transportation Mechanics Analysis

Contents

1. INTRODUCTION

This document presents the mechanics of vibratory handling of microscopic parts. The first part will discuss the basic kinematics of vibration transport. The last part will introduce the effects of adhesion and fluid mechanics.

Vibratory methods provide a promising alternative for transportation of small electronic parts within production and packaging processes. Manipulation, fixturing and transportation are necessary components of any manufacturing process that involves parts produced separately by different processes and then brought together for assembly. As individual parts and assemblies become miniaturized, the techniques used for the corresponding processes at the larger scales are often found to scale unfavorably.

The traditional technique for solving the scaling constraints has been mass parallelization, where groups of small parts are combined in large arrays, and processed simultaneously. A prominent example of this approach is wafer manufacturing of semiconductor devices, where thousands or perhaps millions of distinct parts are processed together on a single wafer, and then separated by die sawing or other methods to yield individual electronic components. In many cases it is found difficult to continue this parallelized approach downstream, where the individual components are no longer attached to each other, and then waffle board or binning methods may be used to provide external structure.

Bulk transport and manipulation methods can be considered as an alternative. These methods are less structured, but if designed appropriately can allow successful parallelization, and alleviate the scaling constraints of individual part transport and manipulation. Such bulk transportation methods are the subject of this paper. The types of functions performed by such a system may be a combination of the following:

- **Transportation:** defined as motion of parts over distances much greater than the part dimensions.
- **Manipulation and orientation**: defined as motion of parts over distances comparable to part dimensions, including rotations and alignments.
- **Grouping or singulation:** parts may need to be sorted into groups or separated individually from the bulk.
- **Fixturing:** locating parts in the appropriate place for processing operations may be directly related to the type of transportation method employed.
- **Delivery:** of parts to the final locations.

The work described here is to provide a foundation for these functions. In what follows we will describe the kinematics of vibratory techniques, and the effects of adhesive and fluid mechanical forces on small parts. Several other techniques which are not described in this document are simultaneously being developed for singulation, precision delivery, packaging, and electrical interconnection with the antennas and other components. The combination of these techniques promises to significantly improve the economics of small chip packaging processes above that achievable with current industrial practice.

1.1. Previous Work

Vibratory feeding of macroscopic parts is well established in industry and research. Bowl feeders [Boothroyd1991] use combined linear and rotational vibration, causing the parts contained within the bowl to move outwards and hop forward incrementally on the rising circumferential track to accomplish feeding. The track may also contain devices for orientation and selection of the parts.

A few other examples of this avenue of research can be mentioned: Bohringer et al. [Bohringer1995], reported using out of plane vibrations of a surface that gather small parts at the vibration nodes. Time asymmetric in-plane driving waveforms have been reported by Reznik et. al. [Reznik1998] and Quaid [Quaid1998]. They achieve feed rates approaching the forward traveling speed of the surface. Part manipulation techniques using MEMS cilia [Terry2001], AC electrostatic fields [Moesner1995], rollers [Luntz1997], and air flow nozzle arrays [Konishi1994] etc. have also been reported in the literature.

2. KINEMATICS

For net motion of the part relative to the supporting surface, relative motion is required, and this may be made possible by ratcheting action. Ratcheting can be achieved by a number of methods:

a) asymmetric in-plane waveforms that utilize symmetric Coulomb sliding friction saturating during part of the cycle;
b) using out of plane waveforms to generate hopping motions that eliminate frictional impulse during the part of the cycle that the surface moves backwards;
c) surface treatments to make the coefficient of friction directional;
d) ultrasonic vibrations or air injection etc. to vary friction during part of the cycle.

Vibratory transportation uses the nonlinear characteristics of Coulomb friction. To move a part relative to a surface, directional slip needs to occur. We can achieve this asymmetric slip through the use of special waveforms or by varying the effective Coulomb friction. We briefly describe the in-plane and out of plane methods below.

2.1. In-plane Surface Motion

Reznik et. al. [Reznik1998] and Quaid [Quaid1998] describe asymmetric in-plane waveforms that use a single actuator to achieve ratcheting. The acceleration diagrams of the Stick-slip waveform and the Coulomb pump are shown in Figure 1 and Figure 2 respectively. The motions are also shown in the graphs in Figure 3.

The gravity friction cone, shown shaded gray in the diagram, allows us to integrate the vertical and horizontal acceleration with the Coulomb friction characteristics. The part's motion must always lie on or inside the friction cone boundary. Wherever the surface's motion is outside the friction cone boundary, the part's motion will saturate. The saturation can occur both horizontally, where horizontal acceleration does not exceed the product of vertical acceleration and μ, and vertically where the downwards acceleration of the part does not exceed g, since it is only gravity that pushes the part against the surface. The externally applied forces on the part such as the force of adhesion or fluid mechanical forces can modify the envelope as we shall see later. The surface moves along the thin lines and filled circles in Figure 1, and the part's acceleration is shown by the ovals. The transitions shown by the arrows and in this case the transitions are instantaneous.

Figure 1: In-plane motion achieved by the stick slip asymmetric waveform; the surface deceleration B (shown by the filled blue circles), is greater than that sustainable by the Coulomb friction on the part B' (shown as white ovals). The surface spends more time accelerating forwards (A) than backwards (B).

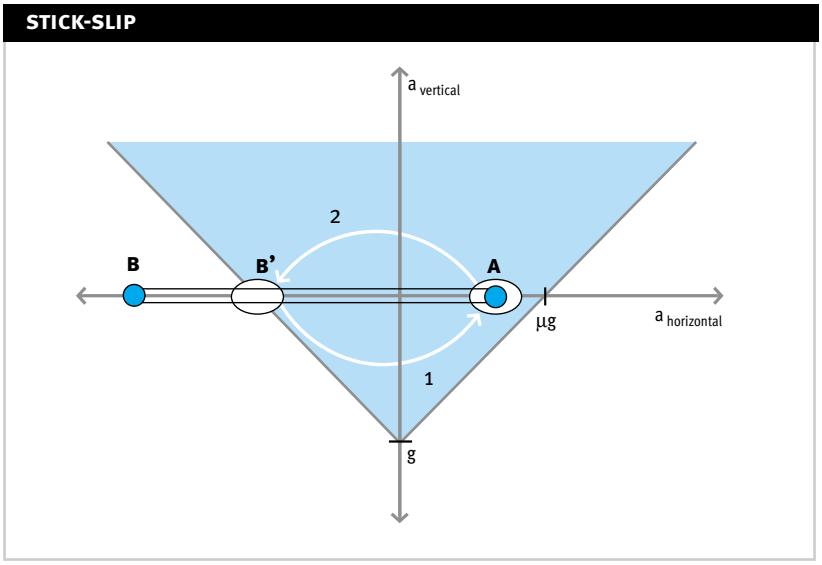

Figure 2: In-plane motion achieved by the Coulomb Pump asymmetric waveform: the surface has accelerations B & C (shown by filled blue circles), greater than that sustainable part due to Coulomb friction B' and C' (white ovals) =. The surface spends more time moving forward (mostly constant velocity at A) then decelerates quickly (B); moves backwards and then reaccelerates (C) to achieve ratcheting motion of the parts.

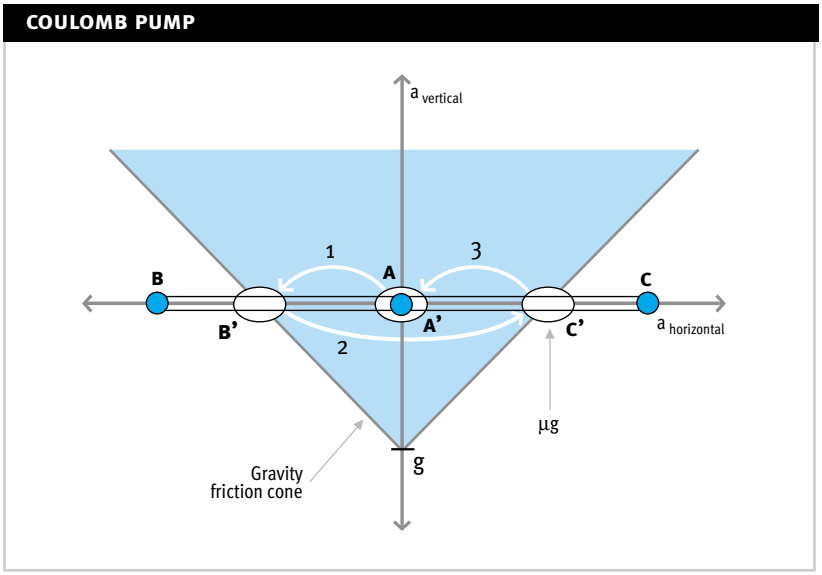

Figure 3a: Asymmetric In-plane waveforms: Stick-Slip and Coulomb pump waveforms shown with accelerations (left), velocities (top right) and position (bottom right). The coulomb friction saturation allows forward motion of the part relative to the surface.

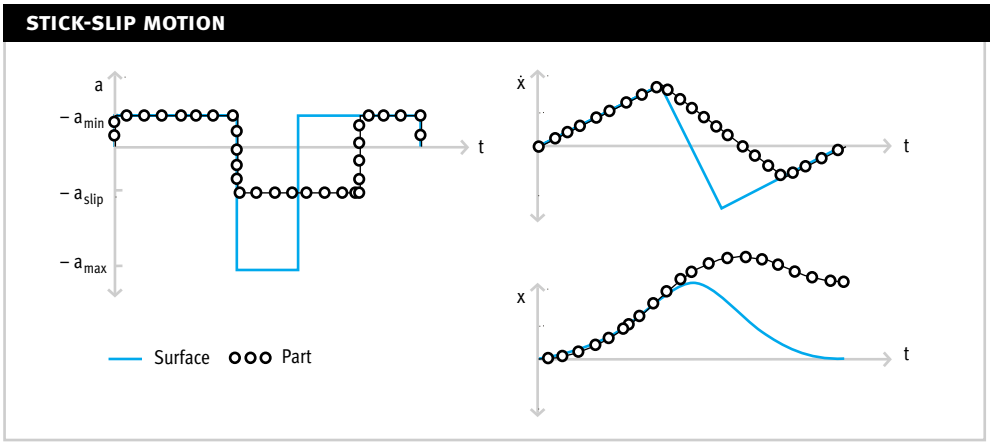

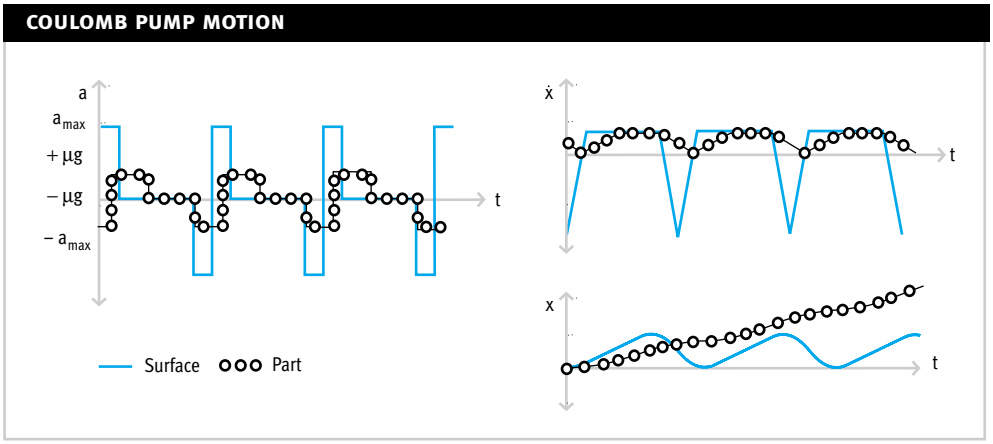

Figure 3a: Asymmetric In-plane waveforms: Stick-Slip and Coulomb pump waveforms shown with accelerations (left), velocities (top right) and position (bottom right). The coulomb friction saturation allows forward motion of the part relative to the surface.

As can be seen, the forward velocity of the part is a fraction of the peak forward velocity of the plate. This fraction can be optimized according to the actuator capability. If impulsive backwards and forwards acceleration of the surface is possible then they can be made equal. However for practical implementations with limited actuator power, one will have to live with a forward motion average that is a fraction of the forward velocity.

2.2. Out-of-plane Motion

As mentioned before, the Coulomb frictional force is dependent on the sign of the part's velocity relative to the plate, and on the normal force between the part and the surface. Out of plane vibrations allow variation of the normal force, and consequently the saturation acceleration level. If we control the plate's oscillatory motion in the vertical direction, such that it is accelerating upwards when accelerating forward, and accelerating downwards when accelerating backwards, then we can also achieve forward motion.

A part initially at rest on the plate's surface will experience a net forwards force of magnitude $\mu m g_f$, which will be greater than the force on the opposite direction $\mu m g_b$, since $g_f > g_b$, resulting in net a forward momentum added to the part after the cycle. The part converges to an average terminal velocity (the feed rate), that depends on both physical friction and actuation characteristics.

The instantaneous acceleration of the surface under the action of a force actuator is given by

$$a = f_{ext}/m_s$$

where m_s is the mass of the surface and f_{ext} is the applied force. Employing direct control over force f_{ext} exerted by the force actuators we can impose an arbitrary acceleration profiles independently in the vertical and horizontal axes. Bowl feeders generally have a single actuator that acts on an axis at an inclination to the surface. Multiple axis actuation offers the possibility of greater sophistication and flexibility.

2.2.1. Sub-hopping Translation

As we increase the horizontal surface motion, the parts move along until they reach the limiting threshold of Coulomb friction $a_{hor} = m_g$. At accelerations faster than this the parts slide and the force on the part while slipping along the surface is determined by the dynamic coulomb friction coefficient and the vertical acceleration:

$$f_{friction} = \mu f_{normal} \, sgn [v_s(t) - v_p(t)]$$

$$f_{normal} = m (g + a_{ys}) \cos ß, \quad when \; g + a_{ys} > 0, \; or$$

$$0, \quad when \; g + a_{ys} \leq 0$$

Where m is the coefficient of friction; m is the mass of the part; g is the vertical acceleration due to gravity; a_{ys} is the vertical acceleration of the surface; v_s and v_p are respectively the velocities of the surface and the part measured parallel to the surface; and b is the inclination of the surface from horizontal. This friction force acts in the direction opposite to the relative velocity. If the surface accelerates downwards faster than gravity, the parts will depart from the surface, and no friction force will be present. For small vertical acceleration amplitudes ($\ddot{y}_s < |g|$), forward motion may still be obtained without hopping. We can see that this is possible if more slipping happens when the surface is accelerating downwards and backwards, and less slipping in the upwards and forward direction. We illustrate a simple example of a square acceleration waveform in the vertical and horizontal directions (both less than g and μ g respectively), with surface inclination $ß = 0$, as shown in Figure 4 and Figure 5.

In Figure 4 the frictional envelope is drawn for a horizontal surface ($ß = 0$). For surfaces with inclination $ß \neq 0$ to the horizontal, the envelope is rotated by the same angle ß around the – g point on the vertical axis.

In Figure 4 we see the constant surface accelerations (in vertical and horizontal axes) at points A and B. The vertical acceleration is of smaller magnitude than gravity, to prevent any hopping and is shown with filled circles. Starting at point A the part moves along with the surface as we are within the friction envelope (shown shaded). Then the surface transitions instantaneously to point B, and the vertical and horizontal accelerations are reversed ($\ddot{y}_s \leq |g|$). The horizontal acceleration of the surface at B is greater than that sustainable by friction, so the part slides relative to the surface and experiences the sliding friction acceleration represented by point B', at the edge of the envelope.

As the vertical and horizontal accelerations of the surface transition and change sign again (back to A), the part is left with a horizontal velocity difference and continues slipping. The part at the transition goes to point A' (to match the vertical acceleration) and slows down until the horizontal velocity difference vanishes. At the point where the velocities match, the part returns to A to begin the cycle once more. Thus even though vertical acceleration of the surface never exceeds the magnitude of gravity, and

Figure 4: Sub-hopping: Accelerations of the surface (filled circles) and parts (hollow ovals). The acceleration of the horizontal surface $ß = 0$ follows a square waveform (points A and B) on both axes. The vertical amplitude of the surface acceleration is less than g. When the surface accelerates downwards and backwards (point B), the acceleration of the part saturates (point B'). The part stays in contact with the surface at all times; are shown by the filled circles. The acceleration of the parts is shown with the hollow circles.

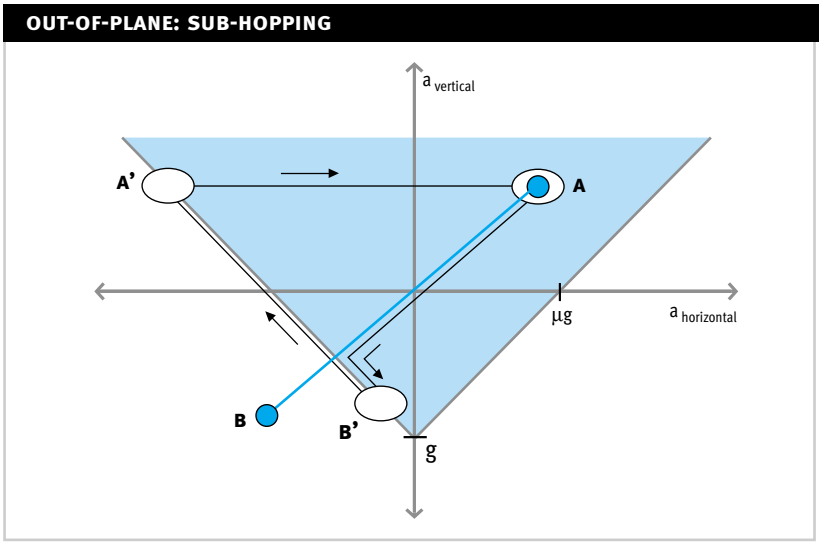

the part follows the vertical motion of the surface always staying in contact, net motion occurs in the horizontal direction.

We can see this horizontal motion more clearly in Figure 5. The symmetric waveform of the surface is translated into the asymmetric one experienced by the part, due to the vertical non-linearity of Coulomb friction, and results in net positive velocity of the part as shown by the hollow circles in Figure 5. The initial transients are quickly damped out and the part motion converges to an average forward velocity.

Figure 5: Simulated motion of the surface and part for square wave accelerations as in Figure 4.

OUT-OF-PLANE: SUB-HOPPING MOTION

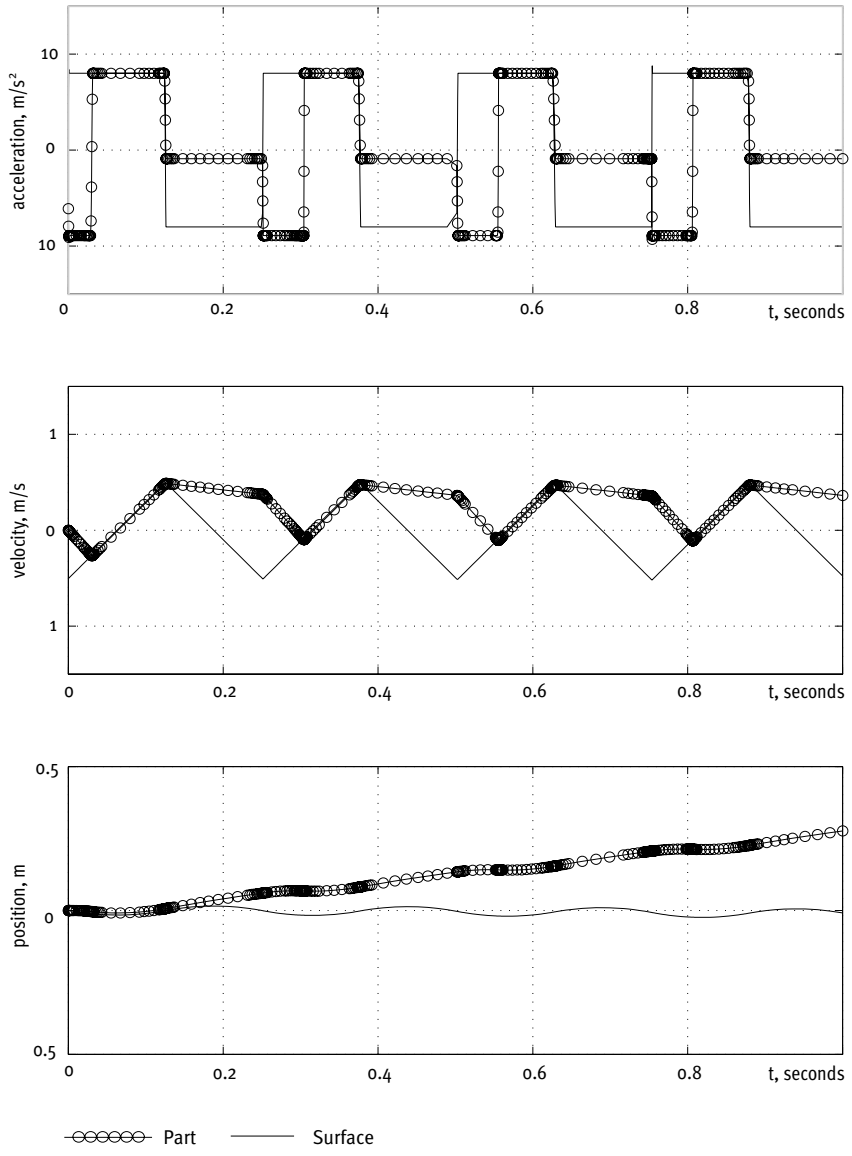

In Figure 6 we show an example of such a condition where the surface is inclined upwards *(ß > 0)* and the parts climb up the incline. Hopping does not occur as the vertical acceleration stays smaller than g, but the deceleration rate is increased because of the adverse inclination. We can also see that if *ß* were to become negative, we could sustain higher horizontal accelerations without slipping backwards.

Figure 6: Sub-hopping: as in Figure 4 except for positive surface inclination rather than zero *ß*.

INCLINED OUT-OF-PLANE SUB-HOPPING

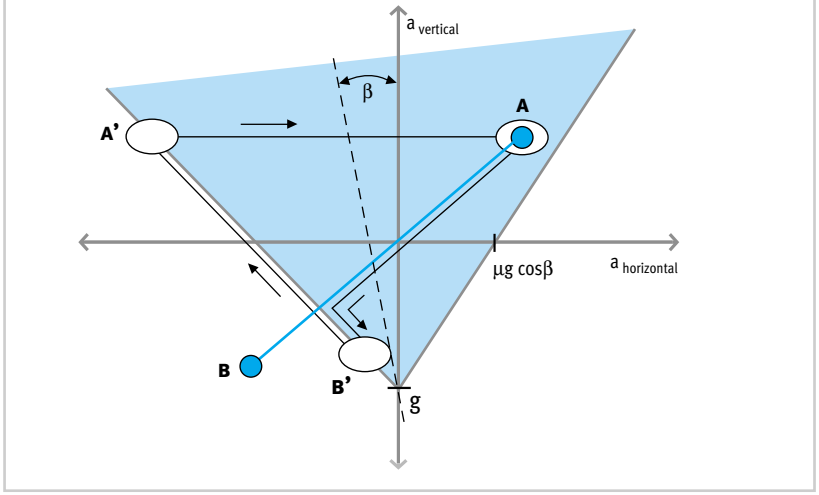

2.2.2. Hopping translation

As we gradually increase the amplitude of vertical acceleration to greater than gravity (in the absence of adhesion), the parts leave the surface in hops. The downwards acceleration of the part cannot exceed gravity at any time, and the part leaves the surface as soon as it exceeds this value. The subsequent impact can be predicted by taking into account the velocity and height of the launch point.

The impact characteristics of the surfaces and the medium determine the degree of elasticity of the collision. The assumption of complete inelasticity is a reasonable simplification for the small scales and relative velocities for our application. This assumption considerably simplifies the analysis as it allows us to discard information about the previous hops. In the case of elastic collisions the previous history must be included in the analysis.

We examine first the case where the vertical acceleration amplitude of the surface is slightly greater than gravity (square wave excitation). In Figure 7 at point A, the part is moving with the surface staying within the Coulomb friction envelope, and accelerating upwards and forwards. As the surface acceleration transitions to the backwards and downwards direction shown by point B, the part loses contact with the surface since the downwards acceleration of the part is limited to –g. The part continues with the horizontal velocity at the time of breaking contact following a free fall trajectory (point B'). When the surface returns to point A, distance remains between it and the part and the part continues at B' until some time later the part makes contact with the surface, shown figuratively as point A'. With the assumption of plastic collisions, an impulse is given to the part in both vertical and horizontal directions tending to eliminate the difference. The vertical impulse equalizes the vertical velocity of the part with the surface. The horizontal impulse does the same for the horizontal axis but does so more slowly. This point is shown figuratively as point A'. The actual position of the point depends upon the surface rigidity and the contact behavior and will normally lie much farther in the left half-plane on the boundary of the friction cone.

The real impact mechanism is likely much more complicated than the simple representation by point A' shown here. The path the part takes in going from point A' to A to re-enter the cycle also depends on the impact mechanics. As shown the return from point A' to A equalizes the vertical velocity first, with no backwards overshoot, and equalizes the horizontal velocity second. This treatment then captures the qualitative aspect of the inelastic collisions in a limited sense. We will return to the frictional impact mechanics question later.

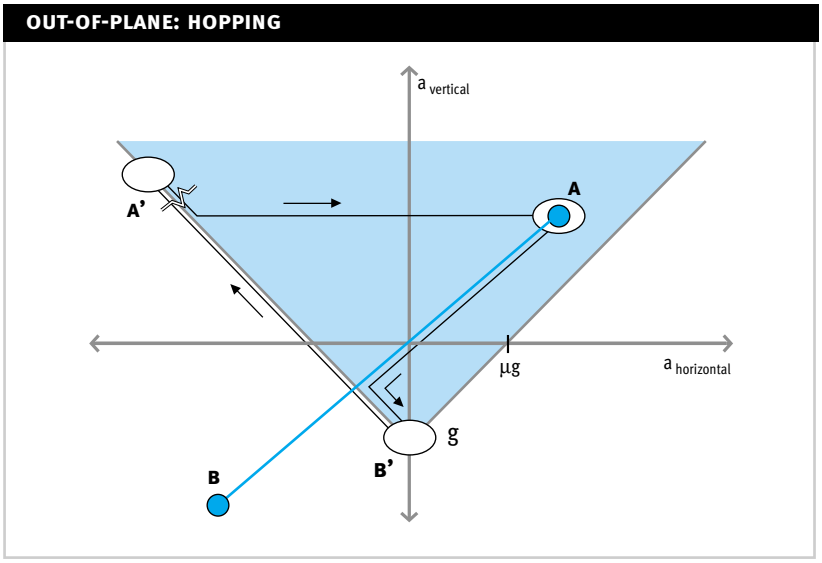

Figure 7: Hopping motion: Accelerations of the surface (filled circles) and part (hollow ovals) for negative vertical accelerations greater than gravity. The part loses contact with the surface and follows a gravitational trajectory with zero horizontal acceleration until impulsive impact occurs at point A' and the part slows down, to equalize horizontal velocity. Impact is modeled here with rigid surfaces and completely damped plastic collisions.

2.3. Analysis: Sinusoidal Waveforms

Sinusoidal actuation may be simpler from a mechanical standpoint, than square wave actuation, especially for higher frequencies, since harmonic drivers can be used.
It is convenient to non-dimensionalize length and time variables for now:

$$\theta = 2\pi t/T_s$$

$$= 2\pi t f_s$$

$$h = 8\pi^2 h_n / [g T_s^2]$$

where θ is dimensionless time; T_s is the fundamental period in normal units; h_n is any length in normal units; h dimensionless length; and g the acceleration due to gravity in normal units. In these non-dimensionalized units gravity g is numerically equal to 2.

For a surface moving according to $h_s = A \sin \theta$, the acceleration felt by the particle while on the surface is $a_p = -A \sin \theta$. The particle leaves the surface when this acceleration exceeds gravity i.e. $a_p < -2$, and time $\theta_l = \sin^{-1}(2/A)$. At that moment the velocity, $V_p = A \cos \theta_l$. The subsequent trajectory under the influence of gravity is described by:

$$h_p(\theta) = A \sin \theta_l + (\theta - \theta_l) A \cos \theta_l + (\theta - \theta_l)^2$$

The peak height achieved above the mean position of the surface is:

$$h_{max} = A \sin \theta_l + (A^2 \cos^2 \theta_l) / 4$$

Assuming inelastic collisions, any impact in the time where the surface acceleration $as < -2$, will result in the particle being launched immediately. For landings at other times the particle will remain on the surface until this condition is met.

The next impact occurs when:

$$h_s = h_p$$

$$A \sin \theta = A \sin \theta_l + (\theta - \theta_l) A \cos \theta_l + (\theta - \theta_l)^2$$

The non-dimensionalized units are found useful for mapping out the types of relative motion that may occur. Vibrations that have identical values of A will have identical peak surface and part accelerations and the motion will be similar

We can relate the amplitude and frequency for a given value of A:

$$Amplitude = [A\, g] / [8 \pi^2\, frequency^2]$$

Next we consider the mechanics as we increase the amplitude A of surface vibration.

2.3.1. Sinusoidal Sub-hopping: $A < g$

Moving the surface periodically in the vertical axis allows us to modulate the effective value of normal inertial force between the part and the surface. For a surface moving according to

$$a_{xs} = A \sin \theta$$

$$a_{ys} = B \sin (\theta + \delta)$$

where a_{xs} is the horizontal acceleration of the surface, δ is the phase lag and a_{ys} is the vertical acceleration.

Sinusoidal waveforms lead to accelerations of the plate that take all values up to the amplitude. For vertical amplitudes less than gravity the behavior is described by the lines in Figure 4, and the circles and ovals represent the peak accelerations. Starting from point A the part moves with the surface until it reaches the edge of frictional envelope. As the downwards and backwards acceleration increases further the part's acceleration is limited to the edge of the envelope. The peak values are shown by points B (surface) and B'(part). Leaving point B and B' the vertical acceleration of the part remains identical to that of the surface, while the horizontal acceleration stays limited to the left bottom edge of the frictional envelope as long as the part is moving faster than the surface. At a time between B' and A' the velocity difference vanishes, and the part returns from the B'–A' line to the A–B line. The exact moment of the snap back can be determined through simulations, such as shown in Figure 8, which shows the horizontal motion variables of the surface (solid lines) and the part (circles). The "snap-back" from negative acceleration to positive acceleration is clearly seen in the acceleration diagram at the top graph of Figure 8.

From the velocity graph of Figure 8, we can observe that the mean velocity of the part is positive and relative motion of the part (bottom graph) to the surface is obtained as in the bottom graph.

OUT-OF-PLANE: SINUSOIDAL SUB-HOPPING MOTION

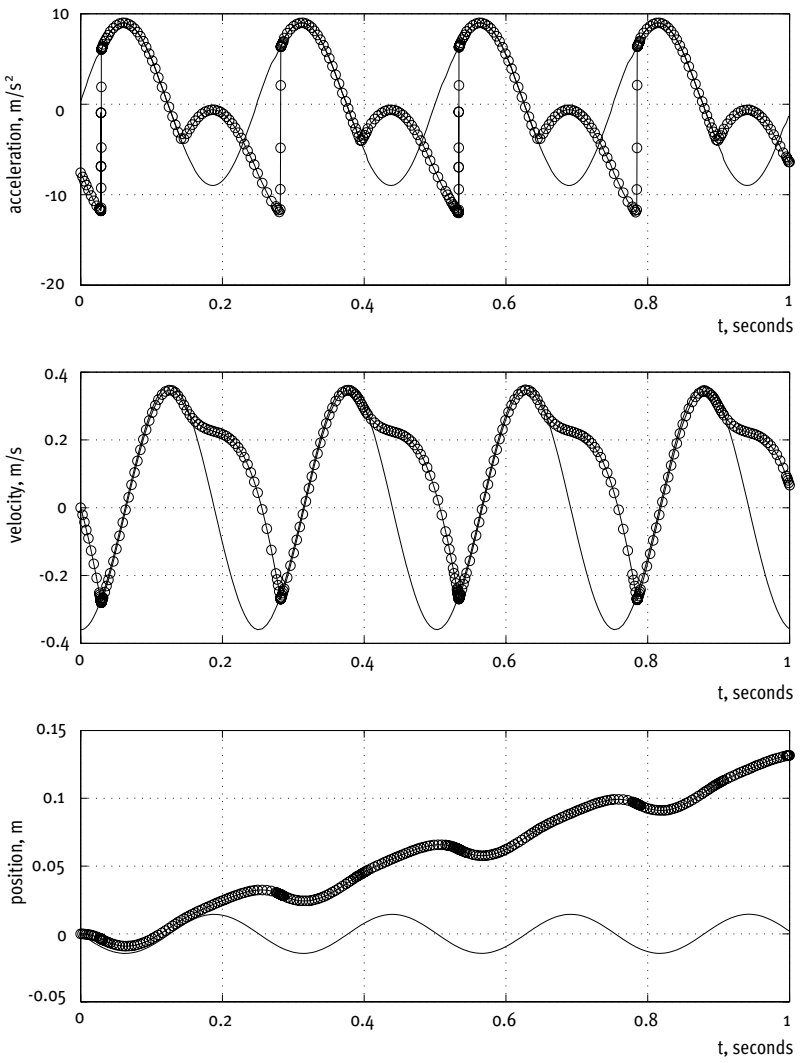

Figure 8: Simulated motion of the surface and part, for pure inclined sinusoidal motion of the surface, *(δ=0), A=1.6, μ=.75,* and a_{ys} *max=.8g*

Comparing the action of these waveforms with the stick slip and Coulomb pump waveforms we note that even without actual hopping, average part velocities close to the maximum forward velocity of the plate can be achieved. As may be expected, given the non-hopping constraint, the peak velocity is achieved when the vertical return acceleration becomes equal to g. This underscores the benefit of out of plane accelerations in reducing friction in the forward motion direction. We may also notice that this can be achieved without requiring asymmetric waveforms, which would require more complicated actuation requirements.

2.3.2. Sinusoidal Hopping: $A > g$

With the surface acceleration amplitude to greater than g in the absence of adhesive forces, the parts enter flight. The initial separation will occur at the rising part of the cycle before the peak. Looking at the solid lines in Figure 7, we see that some slipping must occur before the part separates from the surface. The part impacts the surface again some time later. If the coefficient of restitution is greater than zero then some of the energy may be returned to the object causing it to bounce again.

For zero coefficient of restitution, if the impact occurs while the surface is accelerating at $a_{ys} \geq g$ $(g = -9.81\ ms^{-2})$, then the part will stick to the surface till the launch point is reached. For impacts at other times when the surface is accelerating downwards faster than g $(a_{ys} < g)$, the part will rebound immediately, with the velocity of the surface at the time of impact.

These ranges of A that lead to rebound from impacts can be determined a priori. Using values of A that prevent rebounds, lead to precise launches of the consistent vertical velocity, and allows avoidance of chaotic dynamics. If the particle is dropped into a rebounding mode, it will settle into the stable launching mode. The borders of these ranges are those on the positive and negative slopes, and occur at the same height as the launch. In our non-dimensional units that height is equal to the value of g.

The time aloft from the initial launch point determines the type of impact. Rebound impacts will happen if the jump duration (determined by the value of parameter A) is:

$$2n\pi \leq \theta_{jump} \leq 2n\pi + (\pi - 2\theta_{launch})$$

where θ_{jump} is the duration of the jump in non-dimensional time; n is a positive integer; and θ_{launch} is the time from the positive zero crossing to the time the surface crosses g. For other values of A the jump length will be:

$$2n\pi + (\pi - 2\theta_{launch}) \leq \theta_{jump} \leq 2(n+1)\pi$$

At the end of these jumps the impacts will feed into a launch of the same characteristics as the initial launch, and a periodic solution of period $2(n+1)\pi$ will result. We must consider how that periodic solution may be entered as the vibrations will have to either go through all the amplitudes less than the chosen value of A or have the parts dropped on at an arbitrary time.

The values of A that separate the non-rebounding and rebounding solutions are found as follows. At $A = g$ we get the first non-rebounding solution for an infinitesimal jump. As the value of A is made greater the non-rebounding solutions continue until the impact occurs at $a_{ys} = g$ and $\theta_{ln} = \theta_l + 2n\pi$, where n is 1 at the beginning of the next cycle. In this case the impact height is identical to the launch height. For larger values as we mentioned above we get a rebounding solution. The limiting value has flight duration of exactly 2π. Thus the velocity of launch must be:

$$v_{ys} = n\,\pi\,g = A\cos\theta_l$$

since we know already that

$$g = A\sin\theta_l$$

$$\theta_l = \sin^{-1}(g/A)$$

we can solve for the values of A by eliminating θ_l:

$$n\,\pi\,g = A\sqrt{(1 - \sin^2\theta_l)}$$

$$= A\sqrt{(1 - (g/A)^2)}$$

solving for A:

$$A = g\sqrt{(1 + n^2\pi^2)}, \qquad \text{where n = 1, 2, 3, ...}$$

n is the number of periods that are traversed by the flight. The values of A are 6.5938, 12.7245, 18.9554, 25.2122, etc.

Similarly, we can find the values of A where the impact transitions from the rebounding to non-rebounding solution. The time aloft θ_f in such a case is:

$$\theta_f = (2n+1)\,\pi - 2\,\theta_l \text{ , where n = 1, 2, 3, ...}$$

where *n* is the number of full periods that pass during the flight. As before the launch height is equal to the landing height, but there is no physical impact as the velocities and accelerations of the surface and the part become identical at the landing point without need for an impulse from the surface. From symmetry we find that the velocity at launch must be:

$$v_y = \theta\,[\,(2n+1)\,\pi - 2\,\theta_l\,]\,g$$

$$= A \cos\theta_l$$

and as before:

$$\theta_l = \sin^{-1}(g/A)$$

eliminating θ_l from [eq:antisym1] we get:

$$\theta\,[\,(2n+1)\,\pi - 2\sin^{-1}(g/A)\,]\,g - A\sqrt{(1-(g/A)^2)} = 0$$

$$(g/A) - \sin[\,(n+\theta)\,\pi - \sqrt{((A/g)^2 - 1)} = 0$$

This equation is non-algebraic and solutions have to be found numerically.

The left curve in the 3D plot of Figure 9 shows the calculated jump length for values of A between 2 and 20. For values of A between 2 and 6.5938 the jumps are consistently of a single length. For $A = 6.5938\$$ the jump length is exactly 2π. For A slightly greater than this value ($6.5938 < A < \sim 7.5$) the jump length converges to 2π. For larger values of A the jump length bifurcates, and we alternate between a long and a short jump for a bitable periodic motion of twice the period as the surface. As A increases further the first jump is long enough to land in the trough of the second wave and we again get mono-stable solutions.

Behavior similar to that described before occurs with the complexity that now the second jump can be shorter and lead into a third jump. The wavelength multiple values of A are shorter and two jump sequences may be 3 or 4 periods duration.

The ruled surface in Figure 9 shows the evolution of the jump lengths over five bounces. We can see the increase in complexity of jump sequences going from left to right. The curve on the right side of the 3D plot shows the average jump length corrected to the shorter flight time of the smaller jumps. This curve describes the average speed of the part for in-phase actuation in the vertical plane. These values can be scaled by the relative magnitude of the horizontal motion to predict the mean horizontal speed.

For even higher values of A the complexity increases further with multiple jump solutions interspersed with stable solutions. This analysis can be extended to include amplitude and phase noise. Also the effects of multiple frequencies present can be examined. For higher values of A ($A > 40$), the jump behavior exhibits significant complexity. By running extensive simulations one can determine the statistics of jump heights.

We can constrain the value of A to be within the stable regions considerable simplicity if analysis is achieved. In what follows we will often use this simplification to expedite analysis. For practical applications, control of vibration to less than 1% distortion is likely to be difficult. In such cases controlling the motion to be within the deterministic regions will be difficult.

Figure 9: Normalized jump length evolution for various values of A; the curve on the left hand side shows the jump length; the surface in the middle shows the evolution of jump length; the curve on the right hand side shows the approximate unscaled speed.

HOP EVOLUTION AND AVERAGED SPEEDS

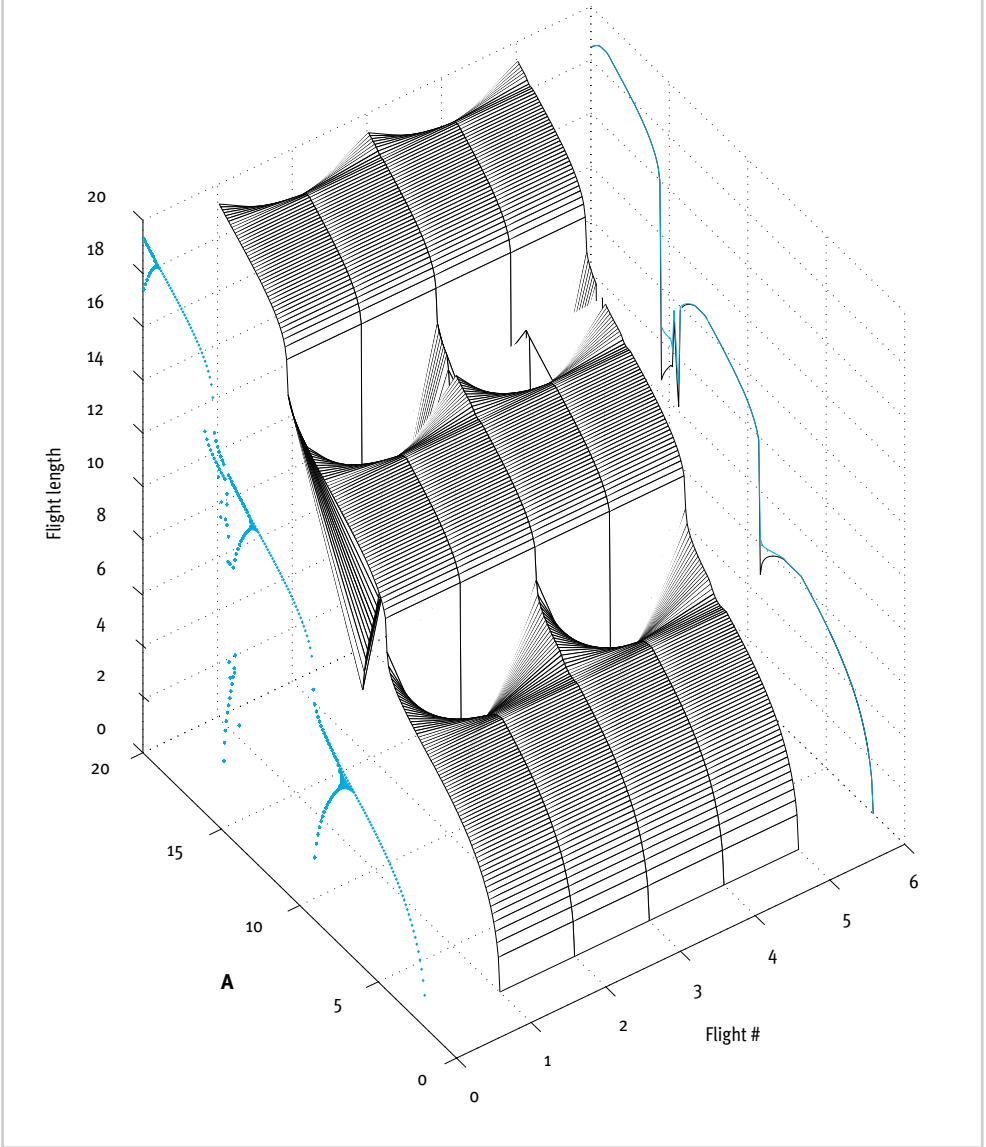

2.4. Phase Optimization

For a given vertical launch velocity, the maximum horizontal motion of the part will be obtained if the launch happens at the peak horizontal velocity of the surface. Horizontal and vertical axis accelerations can be generated with a single linear actuator at an inclination of the surface for in-phase motion, or by independent actuators or other mechanical arrangements if a phase difference is required.

For smaller values of A the parts are launched close to $\theta_1 = \pi/2$ and to have maximum velocity at that point, 90° phase between vertical and horizontal is near optimal. This surface motion in this case would be ellipsoidal. For larger values of A, the parts are launched closer to $\theta_1 = 0$, and the largest horizontal velocity can be obtained if the phase lag is zero. This motion is linear. The near optimality of in phase motion for large values of A is fortunate as it makes mechanical implementation particularly simple. A single inclined actuator can be used to get an average horizontal velocity equivalent to a large fraction of the peak actuation velocity.

3. ADHESION, AND FLUID EFFECTS

Micro-scale and short duration contact friction is an active research topic. Determination of the magnitudes and sensitivities of frictional effects to surface treatments is needed for the design of machines used in processing microscopic parts. As the ratio of part mass to surface area decreases, surface force effects become more prominent. The relative energy dissipated in moving a part on a surface without lifting it off the surface increases in the presence of adhesion. Typical forces that can cause adhesion effects that we may consider are:

– Liquid Capillary forces for wet surfaces.

– Electrostatic forces.

– Van der Waals forces.

For a discussion of these forces see for example [fearing95] and [israelachvili1991]. In what follows we will discuss in particular the effects of van de Waals forces on vibratory transportation. The increase in energy requirements can be estimated.

3.1. Van der Waals Forces

Van der Waals forces play a strong role in intermolecular phenomena. While they are not as strong as ionic electrostatic forces, they are always present. The van der Waals forces between forces are due to static and induced dipoles in materials. The van der Waals potential between two atoms is of the form $w(r) \approx -C/r^6$, and assuming no retardation and linear additive characteristics, we can sum the interactions of all the atoms in one body pair-wise with those in the other to obtain the potential between the two bodies. For a sphere near a surface this potential takes the form:

$$W = -A\,R / 6D \quad [sphere - surface]$$

where A is the Hamaker constant, R is the radius of the sphere and D is the distance from the surface to the edge of the sphere. For a pair of plane surfaces the suitable expression for the potential is:

$$W = -A / (12\,\pi D^2) \quad [surface - surface]$$

The Hamaker constant is simply defined as:

$$A = C\,\rho_1\,\rho_2$$

where ρ_1 and ρ_2 are the number of atoms per unit volume in the two bodies and C is the coefficient and the atom-atom pair-wise potential. A typical value for the Hamaker constant is 10^{-19} J and for condensed phases the Hamaker constants have a range of 0.4 to 4 x 10^{-19} J. Thus for two $100\mu m$ spheres in contact (D = 0.2nm) the adhesion force is $200\ \mu N$ for a Hamaker constant of 10^{-19} J, and the adhesion energy is -10^{-15} Joules. For two planar surfaces separated by the same distance the adhesive pressure will be of the order of 700MPa and the adhesion energy will be -67mJ m^{-2} for the same Hamaker constant.

The energy density of a part launched at velocity v_{yp} is:

$$E_{tot} = \theta \rho v_{yp}^2 \ (in\ J/m^2)$$

where ρ is the areal mass density of the part. For example for a 100 mm thick silicon part launched at $.01\ m\ s^{-1}$, the energy density is about $12\ \mu J\ m^{-2}$. Thus it is obvious we need to reduce the adhesion forces to below this level or use much higher energies. It is in this sense fortunate that most engineering surfaces have contaminants such as dust, and not atomically smooth, so that the practical adhesion pressures and energies are several orders of magnitude smaller than for atomically smooth and clean surfaces. Even at these smaller levels they pose problems at the micro scale. The roughness of the surfaces can be increased and the radii of asperities can be reduced to minimize the contacting surfaces and the consequent adhesive forces and energies. In separating the surfaces, there are other dissipative effects as well such as the viscoelasticity of the materials, elastic waves, and plastic strains during separation, etc. that will also act as energy sinks.

Because of the disparity between the theoretically smooth surfaces and practical rough surfaces, and the difficulty of formulating analytical models for the adhesion of rough multi-asperity surfaces and their contact behavior we have to resort to experimental measurement of adhesion effects for the classes of surfaces and scales we are interested in. Thus far we have done part mobility experiments using plain aluminum surfaces which needed to be grit blasted to increase roughness and permit part movement for parts of about 300 micron scale. Grit blasted surfaces have been see to provide a solution with satisfactory margins against deterioration of motion capability caused by adhesion effect.

We can show the friction cone diagrams used before to describe motion can also to show the effective adhesion. The VdW adhesion can be modeled to first order as a short range energy sink. If the object motion is much larger than the range of VdW adhesion then such a simplification is appropriate.
As an example for the coulomb pump described above, the adhesion friction cone is added as shown in Figure 10 as a cone, which essentially increases the friction envelope. For typical conditions additional pressure in between the surfaces increases the contact area and the adhesion forces increase with increasing pressure. This is illustrated by the slightly larger angle of the adhesion friction cone in Figure 10. The reduction in the acceleration differences between the surface and the parts is apparent, and this leads to reduced motion capability and slower part speeds. The penalty for hopping motion is less severe as the part spends a significant duration outside the adhesion zone.

Figure 10: For in-plane motion net acceleration (distance between C & C') decreases as adhesion increases.

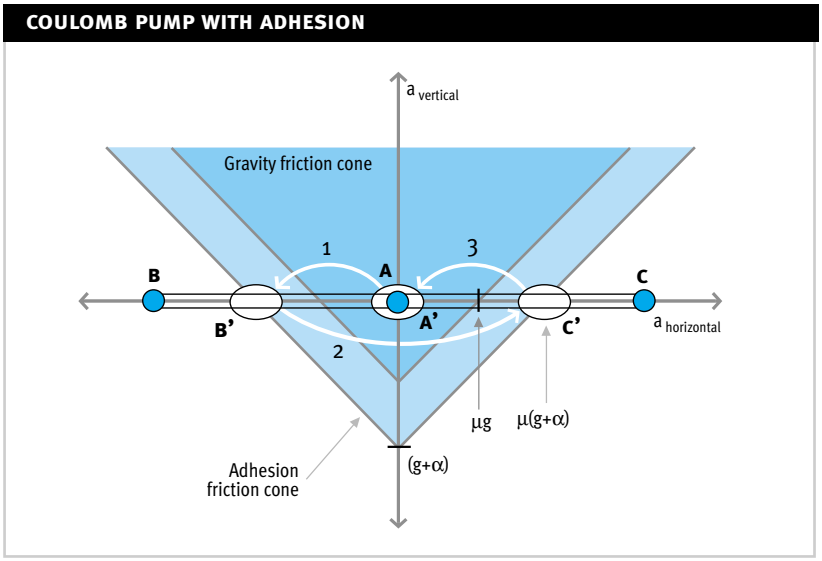

In Figure 11 we show the effect of adhesion for out of plane hopping motion. As the downwards and backwards acceleration increase the part reaches the adhesion limit and slides till the downwards acceleration is greater than what the adhesion can resist. Then the part "snaps-off" to the gravity envelope and into free fall. As the surface returns and meets the part there is a "snap-back" by the adhesion and the part is pulled in going through an adhesive collision and rapidly slowing down till the horizontal velocities are equalized. This motion is similar to the equivalent that would be obtained with an increased gravity except in that the free fall is at normal rate. Adhesion again reduces the motion capacity but the advantage over in-plane motion is sustained. In order to compare actual motion we would need to build a satisfactory model of adhesive collisions and friction, which can become quite involved.

Since our objective is to maximize the horizontal motion, we can contemplate releasing the part from adhesion by using a high g (but low energy and velocity) ultrasonic pulse at the point of maximum horizontal and vertical velocity to release the part. Such hybrid vibration techniques may be utilized as we explore smaller length scales.

Figure 11: For out-of-plane motion the decrease in net acceleration is not as severe as adhesion increases since the part spends a fraction of the time in a zero friction region.

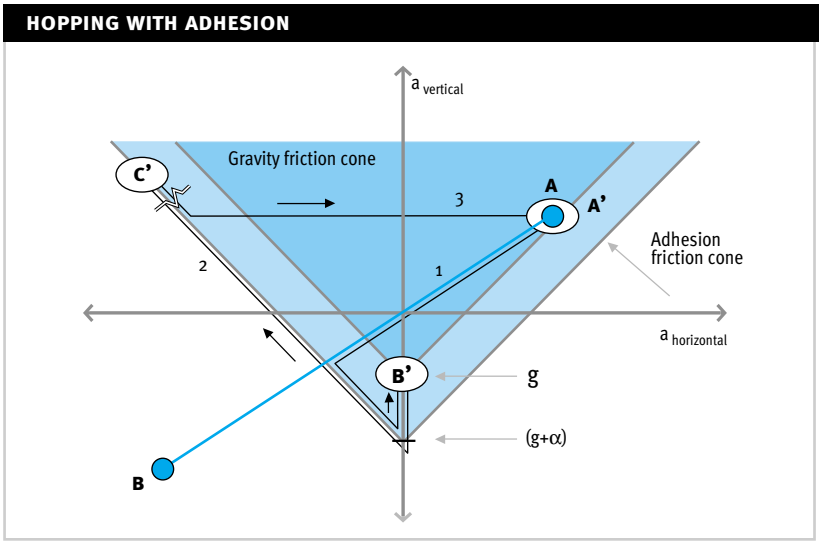

The frequency dependence of VdW adhesion is related to the amount of energy imparted to the part at the point of departure. Higher frequencies for a particular value of A have smaller residual energies, as the velocity decreases with increasing frequency. However since the surface moves away faster, the duration that the attraction is within acting range is also smaller. Since we are interested in hops of tens of microns, the 100 nm range of adhesion can be crossed quickly and the added energy loss can be minimized.

Friction between a surface and an adhering part can also be reduced by applying high acceleration vibrations to a surface. Such an approach was reported by Bohringer et. al. [Bohringer1998]. They reduced adhesion between sputtered gold surfaces, and microelectronic parts by using strong vibrations of the surface in the 20kHz range with measured amplitudes of up to 500nm resulting in vibrations of several hundred g's. The actuator in this case was a piezoelectric stack. This approach neutralizes the additional friction caused by adhesion, and low coefficients of friction can be achieved.

3.2. Fluid Dynamic Scaling

For small distances, Stefan's law gives the force between a static surface and a circular disk being pulled away from it or towards it with some velocity V (Figure 12). Using the standard assumptions (quasi-static, incompressible, laminar flow, no-slip, rigid, parallel smooth surfaces) this force is:

$$F = 1.5 \left(p\, r^4\, \mu V / h^3 \right)$$

Where r is the radius of the disk, m is the viscosity of the fluid, and h is the distance between the surfaces. When the part separates from a vibrating surface this force opposes the motion. At the point of separation the velocities and accelerations of the part and the surface are equal. From that point onwards in the free fall accelerating frame, the surface acceleration increases continuously. If adhesion is absent this acceleration starts from zero, while if adhesion is present this acceleration will start from a nonzero value and will have a more complex profile.

The disk, as it moves away from the surface, will transition from the Stefan's law region to a free flow region. In the scale we are interested in the bounce height will often be significantly smaller than the diameter of the disk (e.g. 40 microns vs. 400). The flow above the surface will move close to the motion of the plate itself, so even away from the plate there will be drag on the disk that will tend to equalize the motion of the disk to that of the surface. The drag force is however small compared with the squeeze film forces for the range of velocities we are interested in. As an illustration the terminal free fall velocities of these silicon disks are of the order of 1 m/s while the peak vibration speeds may be .1 m/s for low frequencies. For such a case the drag contribution to the motion will be small.

Figure 12: Disk receding from surface

DISK RECEDING FROM SURFACE

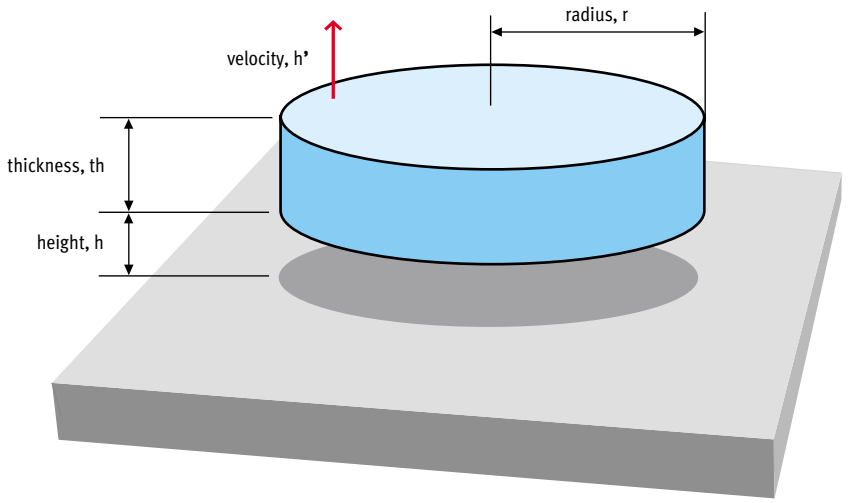

Given an initial small clearance between the part and the surface, we can solve for the motion of the part relative to the surface. For a disk shaped part we can see:

$$h_{yp}'' = 1.5\,\mu\,\pi\,r^4\,(h_{yp}' - h_{ys}')\,/\,[\,m\,(h_{yp} - h_{ys})^3\,]$$

Where m is the mass of the part; hyp and hys are the vertical positions of the part and the surface respectively. If the surface is moving according to:

$$h_{ys}'' = -a\,\omega^2 \sin(\omega t)$$

$$h_{ys}' = a\,\omega \cos(\omega t)$$

$$h_{ys} = a \sin(\omega t)$$

Where a is the amplitude of the vibration and w is the angular velocity. Substituting gives us the nonlinear differential equation:

$$h_{yp}'' = 1.5\,\mu\,\pi\,r^4\,(\,v_{yp} - a\,\omega \cos(\omega t)\,)\,/\,[\,m\,(h_{yp} - a \sin(\omega t))^3\,]$$

Which can be integrated numerically.

In Figure 13 we show an example of the calculated velocity deficit due to thin squeeze film damping for a Silicon disc (400micron diameter and 200 micron thick) being launched by vibration at various distances from the surface for a range of frequencies. The amplitudes of vibrations are scaled with frequency to keep the value of A at a constant 20, (i.e. 10g peak acceleration). At low frequencies the velocity deficit shows frequency dependence. At higher frequencies the deficit approaches the limit for infinitely fast withdrawal of the surface. The no hop region shown is defined by the peak velocity of the surface during the vibration cycle. The actual launched velocity of the part is the vertical difference between this boundary and the velocity deficit curve. The part cannot have a launch velocity deficit greater than the

launch velocity itself since then the launch would not occur. At higher frequencies it is thus possible to have the part continue to stay close to the surface and never get free. The saturated velocity deficit shows an inverse square dependence to stand-off distance. At smaller gaps and large accelerations the assumption of low Mach number may begin to break down, before the ultimate limit of atmospheric pressure is reached.

Figure 13: Velocity deficit for a 400 micron dia. 200 micron thick Silicon disc, for various starting clearances, and frequencies. (Note the magnification in frequency scale between 0 and 3 Hz).

FILM DAMPING VELOCITY DEFICIT

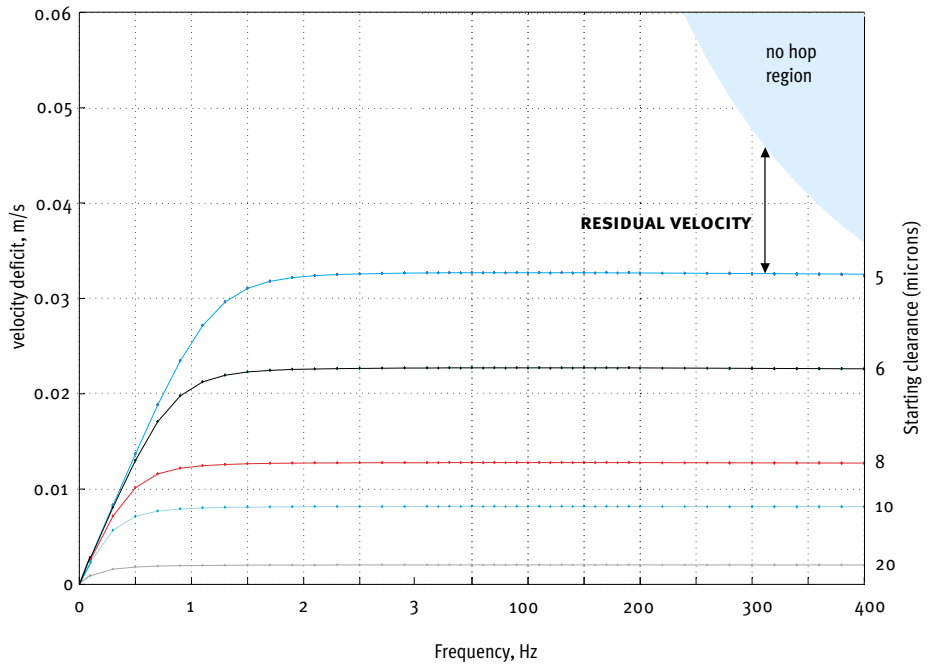

Since the retarding pressure is area dependent, making the part's surface ventilated will significantly reduce air damping effects. Thus to alleviate the fluid damping effects we can roughen or pattern the surfaces so that the asperities become large, increasing the effective stand-off distance, and the fluid damping effects are minimized. Flow through irregular geometries can become very complex. We are also close to the mean free path of air molecules, and below a certain length scale slip effects will become important. Squeeze film characteristics for individual small asperities will likely fall within the slip flow regime. Elasto-hydrodynamic slip flows for hydrophobic surfaces within liquids are discussed by O. Vinogradova [vinogradova2002]. For small asperities the areas will be small, and as we mentioned earlier, the total force will likely be predominated by the VdW pressure, which may be thousands of times larger than the atmospheric pressure.

In summation to alleviate the fluid damping effects, we can increase the clearance between the part and the surface by increasing roughness of the surfaces. Using lower frequencies with higher peak velocities is also advantageous as it allows lower penalty from the velocity deficit, as well as requiring lower actuator bandwidth.

4. CONCLUSIONS

In this article, we presented the introductory development of the theoretical underpinnings of the vibratory methods being considered for use in transportation of microscopic parts. We demonstrated the advantages of out of plane waveforms for the transportation of microscopic parts. We also noted that using surfaces with higher degree of roughness is preferable from both the adhesion and fluid mechanics perspectives.

5. REFERENCES

[Bohringer1995]
1. **K. Bohringer, V. Bhatt & K. Goldberg, "Sensorless manipulation using transverse vibrations of a plate".**
Proc. of the IEEE Int. Conf. on Robotics and Automation (ICRA'95), Nagoya, Japan, May 1995.

[Bohringer1998]
2. **K. Bohringer, K. Goldberg, M. Cohn, R. Howe & A. Pisano, "Parallel microassembly with electrostatic force fields".**
IEEE Int. Conf. on Robotics and Automation (ICRA), Leuven, Belgium, May 1998.

[Boothroyd1991]
3. **G. Boothroyd, "Assembly automation and product design".**
Marcel Dekker Inc. New York, NY, 1991.

[Fearing1995]
4. **R. Fearing, "Survey of sticking effects for micro parts handling".**
IEEE/RSJ Conf. on Intel. Robots and Systems, v. 2, Pittsburgh, PA, 1995, pp. 212–217.

[Israelachvili1991]
5. **J. Israelachvili, "Intermolecular and surface forces".**
Academic Press, London; San Diego 1991, 2 ed.

[Konishi1994]
6. **S. Konishi & H. Fujita, "A conveyance system using air flow".**
IEEE Journal of MEMS, vol. 3, no 2, June 1994, pp. 54–58.

[Luntz1997]
7. **J. Luntz, W. Messner & H. Choset, "Manipulation and dynamics with a distributed actuator array".**
IEEE Robotics and Automation conference, April 1997.

[Moesner1995]
8. **F. Moesner & T. Higuchi, "Devices for particle handling by an ac field".**
IEEE MEMS conference 1995.

[Quaid1998]
9. **A. Quaid, "A miniature mobile parts feeder: Operating principles and simulation results".**
Proc. 1999 IEEE Intl. Conf. on Robotics and Automation, 1998.

[Reznik1998]
10. **D. Reznik & J. Canny, "The coulomb pump: a novel parts feeding method using a horizontally-vibrating surface".**
IEEE Conference on Robotics and Automation, Leuven, Belgium, April 1998, pp. 869–874.

[Terry2001]

11. **M. Terry, J. Reiter, K. Bhringer, J. Suh & G. Kovacs, "A docking system for microsatellites based on mems actuator arrays".**
Smart Mater. Struct., 10 (2001), pp. 1176–1184.

[Vinogradova2002]

12. **O. Vinogradova & F.Feuillebois, "Elastohydrodynamic Collision of Two Spheres Allowing Slip on Their Surfaces".**
J. Collo. Interf. Sci., 2000, V.221, N.1, p.1–12

Designed and produced by Foxner. www.foxner.com